Mechanical Engineering – Scientific Journal, Vol. **43,** No. 1, pp. 49–57 (2025)
Number of article: 693
Received: April 24, 2025
Accepted: May 12, 2025
In print: ISSN 1857–5293
On line: ISSN 1857–9191
UDC: 621.313.13-133.2:534.242.089
https://doi.org/10.55302/MESJ2543149a

Original scientific paper

REAL-TIME VIBRATION ANALYSIS AND RESONANCE DETECTION OF STEPPER MOTORS

Medin Ademi, Maja Anačkova, Dejan Šiškovski

Faculty of Mechanical Engineering, "Ss. Cyril and Methodius" University in Skopje, P.O.Box 464, MK-1001 Skopje, Republic of North Macedonia
m.ademi2607@student.mf.ukim.edu.mk

A b s t r a c t: This paper focuses on developing a real-time system for vibration analysis and resonance detection in stepper motors used in CNC machines. The goal is to optimize motor performance and reduce resonance effects, which impact precision and efficiency. The ADXL345 accelerometer is mounted near the motor shaft to measure vibrations, while the Arduino Mega 2560 serves as an interface. Vibration data is processed in LabVIEW using FFT to analyze frequency and time domains. A potentiometer controls the motor speed, powered by an L298N driver. Additionally, an Arduino Uno reads the potentiometer input and adjusts the speed. The TCST1230 optical sensor measures the motor's RPM, allowing a detailed analysis of the relationship between speed and vibration frequencies. Results visualized in Excel help identify resonance frequencies, enabling better parameter selection. This system enhances the accuracy, efficiency, and longevity of CNC machines by minimizing harmful vibrations.

Key words: resonance detection; CNC machine; accelerometer; FFT; Arduino

РЕАЛНОВРЕМЕНСКА АНАЛИЗА НА ВИБРАЦИИ И ДЕТЕКЦИЈА НА РЕЗОНАНЦИЈА КАЈ ЧЕКОРНИТЕ МОТОРИ

А п с т р а к т: Овој труд се фокусира на развој на реалновременски системи за анализа на вибрации и детекција на резонанција кај чекорните мотори во CNC-машини. Целта е да се оптимизираат перформансите на моторот и да се намалат негативните ефекти од резонанција, која влијае врз прецизноста и ефикасноста. До вратилото на моторот е поставен акцелерометар ADXL345 за мерење вибрации, додека Arduino Mega 2560 служи како интерфејс. Податоците се обработуваат во LabVIEW користејќи FFT за анализа во фреквенциски и временски домен. Потенциометарот ја контролира брзината, додека драјверот L298N го напојува моторот. Дополнително, Arduino Uno го чита сигналот од потенциометарот и ја контролира брзината. Оптичкиот сензор TCST1230 ја мери брзината на моторот RPM, овозможувајќи анализа на врската меѓу брзината и вибрациите. Резултатите во Excel помагаат во идентификација на резонантните фреквенции, овозможувајќи подобар избор на параметрите и намалување на штетните вибрации во CNC-машините.

Клучни зборови: детекција на резонанција; CNC-машина; акцелерометар; FFT; Ардуино

1. INTRODUCTION

Over the years, stepper motors have evolved significantly, with their commercial adoption beginning in the 1960s. This was largely due to advancements in silicon wafer fabrication, which enabled the development of devices capable of switching high DC currents in motor windings. Initially, stepper motors were not considered a viable alternative to AC or DC servomotors because of their limited high-speed performance. However, as noted by Stout (2000), improvements in motor design and drive systems have made stepper motors highly effective actuators in digital control systems. Their operation can be described as inherently digital, as the rotor moves in precise, discrete steps when the motor windings are energized [1].

Stepper motors enable various operating modes, such as Fullstepping, Halfstepping, and Microstepping, which play a crucial role in their use in different applications (CNC machines, robotic arms, 3D printers, etc.). In the context of research on frequency resonance detection, the characteristics of the Fullstepping mode are of particular importance and

will be used in this study. Below Table 1 is a explaining the different operating modes and their characteristics based on the specifications provided in the QSH4218 stepper motor datasheet [2].

T a b l e 1

Different operating modes of stepper motors and their characteristics

Driver scheme	Resolution	Velocity range	Comment
Fullstepping	200 steps per rotation	Low to very high. Skip resonance areas in low to medium velocity range	Audible noise and vibrations especially at low velocities
Halfstepping	200 steps per rotation*2	Low to very high. Skip resonance areas in low to medium velocity range	Audible noise and vibrations especially at low velocities
Microstepping	200*(number of microsteps) per rotation	Low to high	Low noise, smooth motor behavior
Mixed: Microstepping and Fullstepping for high velocitites	200*(number of microsteps) per rotation	Low to very high	At high velocities, there is no audible difference for fullstepping

When a step motor is driven in the open-loop mode, pronounced velocity oscillations are observed in certain input frequency ranges (steps/sec). In the low-frequency range, the step motor exhibits substantial oscillations at or near the natural frequency and its subharmonics. This phenomenon, known as "low-frequency resonance", is well-documented in the literature. According to Higuchi, Mizuno, and Oshima (1981), this resonance occurs due to the interaction between the motor's mechanical inertia and the electromagnetic forces generated during operation [3]. In this study, resonance is detected by comparing the input frequency (derived from the optic sensor measuring RPM) with the vibration frequency (measured using the ADXL345 accelerometer). When these frequencies align, the system enters a resonant state, leading to increased vibrations and oscillations, as predicted by the theoretical framework described in [3]. Resonance in stepper motors can significantly affect their stability, particularly at certain speeds, leading to unstable torque output. A common issue in motion control systems is the occurrence of vibrations at low speeds, which become especially pronounced when the motor operates near its resonance frequency. As demonstrated by Arva, Stanica, and Anghel (2018) [4], one of the primary causes of these vibrations is cogging torque, which arises from the interaction between the permanent magnet poles and the stator, generating unwanted oscillations. As the input frequency approaches the motor's natural frequency, the system may initially appear to function normally; however, speed oscillations eventually emerge. This oscillatory behavior typically becomes noticeable at frequencies higher than several hundred steps per second. In the literature, this phenomenon is commonly referred to as "medium frequency resonance" or "high frequency resonance". When the motor operates within its resonance frequency range, a sudden drop in available torque is observed, and the torque does not recover to its previous level. This effect, referred to as a torque drop on the torque-speed curve, severely limits the motor's operational performance [4]. Additionally, Kenjo and Sugawara (1994) [5] highlight that the resonance phenomenon is exacerbated by the nonlinear dynamics of the motor's rotor-stator interaction, particularly in open-loop control systems where feedback compensation is absent [5]. In the context of CNC machines, resonance can have detrimental effects on machining accuracy and surface finish. As noted by Altintas and Weck (2004) [6], vibrations caused by resonance in stepper motors can propagate through the machine structure, leading to chatter and poor surface quality in machined parts [6]. This is particularly critical in high-precision CNC applications, where even minor oscillations can result in dimensional inaccuracies and increased tool wear. Smith et al. (2020) [14] further emphasize that resonance-induced vibrations in CNC systems can lead to reduced machining efficiency and higher energy consumption, highlighting the need for effective resonance suppression techniques [7].

The study underscores the importance of mitigating resonance in CNC systems to ensure optimal performance and product quality. The present paper is structured as follows: The second section presents the operating mode and connections required to drive the stepper motor. The third section explains the selection of the sensor. The fourth section presents the experimental setup and experimental results, while the final section is reserved for conclusions.

2. STEPPER MOTOR CONNECTIONS

a) *Stepper motor calculations*

The stepper motor's behavior is a critical factor in the Arduino coding process, and its implementation depends on the specific type of motor selected. As described in the research by Harun and Lim, to calculate the number of steps required for the motor to complete one full revolution, the following equation is used. For most standard stepper motors, the step angle is 1.8 degrees per step, which translates to 200 steps per revolution [8].

$$\frac{360\ Degree}{1\ Revolution\ \frac{Degree}{Step}} = \frac{Step}{Revolution}$$

As mentioned at the beginning, there are different operating modes for the stepper motor, but for the purpose of this study, we use the mode that is most suitable for vibration detection and frequency resonance analysis, which is the Full-step mode. This operating mode ensures a constant angular position of 1.8° per step. In our case, with an angle of 1.8° per step, the number of steps per revolution will be:

$$\frac{360°}{1{,}8\,°} = 200\ steps/revolution$$

For this research, a NEMA17 stepper motor (model QSH4218-35-10-027) was utilized. According to the datasheet documentation (see Figure 1), the wiring layout and the configuration of the two windings were identified, which is critical for ensuring correct motor connections.

Fig. 1. Documentation of the datasheet for stepper motor NEMA17 QSH4218-35-10-027

The motor is equipped with UL 1007 wires, which have a thickness of AWG26. This wire specification is vital for maintaining sufficient electrical conductivity and minimizing resistance within the system. These parameters are particularly significant in this study, as proper electrical connectivity and reduced losses are essential for obtaining precise motor speed measurements [9].

b) *Stepper motor connections*

One of the critical aspects of stepper motor applications is the selection of a suitable driver for motor control. Operating a stepper motor involves switching the current between the stator windings, a function managed by the driver, which regulates and amplifies the control pulses. For this study, the L298N driver was integrated to power the motor, serving as the central component of the motion control hardware system. Based on the methodology outlined in Muain (2010) [10], the L298N driver acted as a power interface, enabling synchronization between the microcontroller and the NEMA17 stepper motor. Powered by a 12 V and 2 A adapter, the L298N efficiently regulated and amplified the voltage and current, ensuring optimal motor performance. The motor windings were connected to the designated A and B pins on the L298N driver, following the connection scheme described in Muain (2010). Additionally, the control pins were carefully linked to the corresponding pins on the Arduino, establishing a reliable communication pathway. To connect all components, 6 female-to-male jumper wires and 3 male-to-male jumper wires were used. A stable electrical environment was achieved by grounding the negative pins together with the Arduino's ground, as recommended in the referenced research [10]. To control the speed of the stepper motor, a 100 kΩ potentiometer was used, enabling precise speed regulation, which is essential for vibration measurement. In this setup, an Arduino UNO was implemented, powered via an adapter, and served as the central control unit for managing the motor's operation. The connection diagram, including the L298N driver, stepper motor, potentiometer, and all necessary pins from the Arduino UNO, is shown in Figure 2.

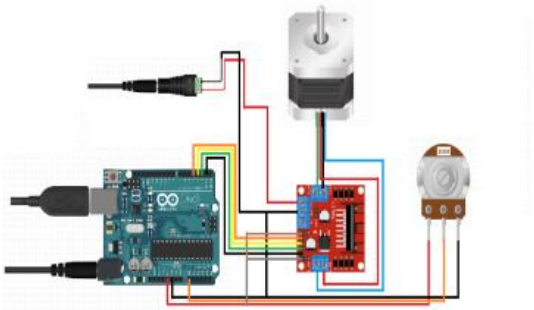

Fig. 2. Connection diagram of the stepper motor, L298N driver, Arduino UNO, and potentiometer

3. ADXL345 ACCELEROMETER

The selection of the sensor is crucial for achieving accurate results, with requirements for stable performance and a good frequency response. According to the study by Rodrigues et al. (2021) [11], Micro-Electro-Mechanical Systems (MEMS) are microdevices that combine mechanical and electrical properties, creating an interface between mechanical and electronic phenomena at a microscopic level. Accelerometers developed using this technology consist of three main components: (i) a seismic mass, (ii) a system of micro-springs that attach the mass to the circuit substrate, and (iii) a system of multiple parallel plate capacitors. When the seismic mass is subjected to acceleration, the springs allow the lateral plates of the mass to move into the dielectric region of the capacitors. The presence of this material within the electric field causes a variation in the system's capacitance, generating an electrical disturbance that can be detected by measuring the electric current between the plates in an intermediate circuit [11].

The ability of an accelerometer to provide reliable responses under mechanical excitation is determined by five key criteria:

i) Sensitivity, which relates the intensity of the electrical signal (in V) to the amplitude of vibrations;

ii) Frequency range, which defines the range of frequencies supported by the circuit;

iii) Maximum supported vibration amplitude, which indicates the highest vibration level the accelerometer can measure;

iv) Shock limit, which specifies the maximum acceleration the MEMS device can withstand;

v) Linearity, which reflects how well the accelerometer's responses align with a specific mathematical model within the supported frequency range.

The analysis of these characteristics, combined with the implementation costs, is ideal for selecting the most suitable accelerometer for our application. A list of key specifications for the desired application has been established, as shown in Table 2. The acceleration range was determined based on research by Saponara et al. (2015) [12]. The bandwidth, or frequency range, is a critical factor in determining which sensor to use. For digital MEMS sensors, the bandwidth is limited to half the data transmission rate of the signal processing circuit to satisfy the Nyquist frequency criterion. The operating temperature is also significant, as high temperatures can occur during the operational mode of the stepper motor.

T a b l e 2

Desired sensor specification

Specification	Min	Max
Brandwidth	50 Hz	1 kHz
Interface	Digital or analog	N/A
Operating temperature	–10°C	70°C
Acceleration range	0.5 g	5 g
Noise density	Og/√Hz	10 mg/√Hz
Cross axis sensitivity		
Cost	0	$150

With these key characteristics in mind, a selection of commonly available sensors has been evaluated in Table 3. All of these sensors come premounted on development boards that include basic circuitry and connection terminals. They are all designed to function within a temperature range of -40°C to +85°C, making them well-suited for the intended application.

T a b l e 3

Comparison of MEMS sensors for vibration measurement

Sensor	Band. width. Hz	Interface	Noise density mg/√Hz	Cost ($)
ADXL345	6.25 to 1600	SPI / I2C	3.9 31.2	84
ADXL343	0.1 to 1600	SPI	4.2 34.3	60
ADIS16209	0 to 50	SPI	0.19	161
ADXL375	0 to 1000	SPI / I2C	5	60
LIS331AL	0 to 1000	Analog	0.3	71
BMA150	25 to 1500	I2C	0.5	42

From the analyzed MEMS sensors, the most suitable for measuring vibrations on a stepper motor is the ADXL345, as it meets all the required criteria. The ADXL345 (Figure 3) is a compact 3 mm × 5 mm × 1 mm device with a selectable measurement range of ±2 g, ±4 g, ±8 g, and ±16 g. For this application,

the ±2 g range is used, as it offers the highest resolution, which is ideal for detecting small vibrations in the stepper motor. It features a 32 level FIFO buffer, reducing microcontroller interaction and saving power. The block diagram below shows the 3 axis MEMS sensor, ADC, digital filter, and FIFO buffer. It supports SPI and I2C communication, has interrupt logic for event detection, and includes a power management system for efficient operation.

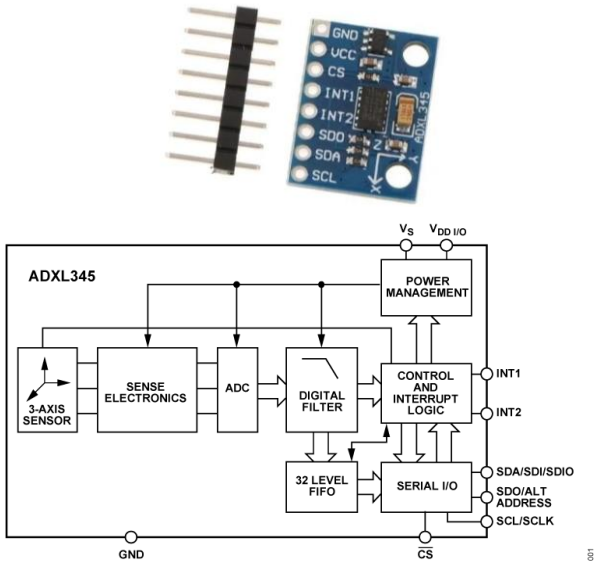

Fig. 3. ADXL345 sensor module and block diagram

4. EXPERIMENTAL SETUP

a) *Hardware setup and description*

The hardware setup shown in Figure 4 consists of a stepper motor (NEMA17), Arduino UNO, Arduino mega 2560, L298N driver, ADXL345 and TCST1230 optic sensor. The optical sensor is mounted on one of the mounting holes of the stepper motor to measure RPM. A metal disk with a hole is attached to the motor shaft, and the optical sensor detects this hole to monitor the rotational movement. Additionally, the ADXL345 accelerometer is mounted on the other mounting hole of the stepper motor, allowing it to capture more accurate data for the RPM measurement. The experimental setup works as follows: The Arduino Mega 2560 is responsible for signal processing through LabVIEW. It communicates with the sensors via the SDA and SCL pins, collecting data from both the optical sensor (for RPM measurement) and the ADXL345 accelerometer (for more precise motion data). The data is processed in LabVIEW using FFT blocks to analyze the signals in both the time and frequency domains. This enables the display of RPM and other relevant metrics on the LabVIEW front panel. The Arduino UNO is used to drive the stepper motor, with a potentiometer allowing the motor's speed to be varied from minimum to maximum in order to detect resonance frequencies. The optical sensor monitors the RPM, which is then displayed on the LabVIEW front panel through a gauge.

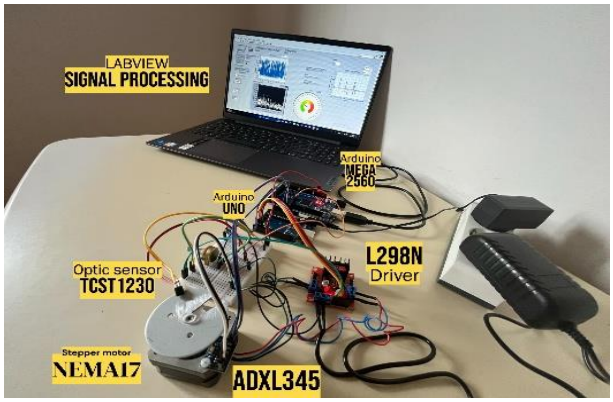

Fig. 4. Hardware setup

b) *Signal processing and FFT implementation in LabVIEW*

For measuring the vibrations of a stepper motor using LabVIEW and Arduino Mega 2560, the Fast Fourier Transform (FFT) is essential for signal processing. Several parameters in the Virtual Instrument (VI) play a key role in obtaining accurate measurements. The sampling frequency (f_s) defines the number of measurements or samples taken per unit of time during the digitization of the analog signal, and it must be greater than twice the highest frequency of the vibration signal to avoid aliasing (false frequency). The FFT size (N) determines the number of points used for the FFT calculation, directly affecting both the frequency resolution (Δf) and the computational load. Specifically, a larger FFT size allows for a finer frequency resolution, but it also demands more computation time. For example, when the sampling frequency (f_s) is set to 3.7 Hz and the FFT size (N) is 1024, the frequency resolution is calculated as shown in the literature by National Instruments (2020), where the relationship between f_s, N, and frequency resolution is described in detail [13].

$$\Delta f = \frac{f_s}{N} = \frac{3{,}7}{1024} = 0.00361 \text{ Hz}$$

This implies that we can distinguish frequencies with very small differences, which is particularly important when analyzing vibrations with closely spaced frequency components. The chosen

parameters f_s = 3.7 Hz and N =1024 are suitable because they provide sufficiently high resolution for analyzing the vibrations of the stepper motor, whose operating frequency ranges from 0 to 1.8 Hz. The sampling frequency f_s = 3.7 Hz is greater than twice the highest frequency of the signal (1.8 Hz × 2 = 3.6 Hz), meaning it satisfies the Sampling Theorem and ensures accurate reconstruction of the signal's frequency components without aliasing. With this configuration, the stepper motor's vibrations can be precisely analyzed in both the time domain using the Time Graph and in the frequency domain using the Frequency Graph.

5. RESULTS AND DISCUSSION

a) *Vibration analysis along the X-axis*

In the experimental setup, the ADXL345 accelerometer is mounted on the stepper motor's mounting hole, with its *X* and *Y* axes aligned horizontally, while the *Z*-axis is oriented vertically. Exeriments were first conducted at lower speeds, 20 and 40 RPM, to analyze resonance effects. At these speeds, resonance was detected, causing the motor to stop due to mechanical instability. FFT analysis shown in Figure 5 revealed resonant frequencies of 1.40 Hz (20 RPM) and 1.60 Hz (40 RPM), while the calculated rotational frequencies of the motor were 0.30 Hz and 0.67 Hz, respectively. This occurred due to the alignment of natural vibration frequencies with harmonics generated by the motor's rotation, amplifying vibrations and leading to instability. Figure 5 also shows amplified vibrations in the time domain, particularly along the *X*-axis, further confirming the presence of resonance. These data clearly indicate that at 20 RPM and 40 RPM, the system enters a critical operating mode, leading to significant mechanical disturbances and motor stoppage. Meanwhile experiments at higher speeds were also conducted, 60 and 120 RPM, where the frequency graph revealed dominant frequency which exactly matched the calculated rotational frequency. Unlike the previous speeds where resonance occurred, this time the motor continued to operate without interruptions.

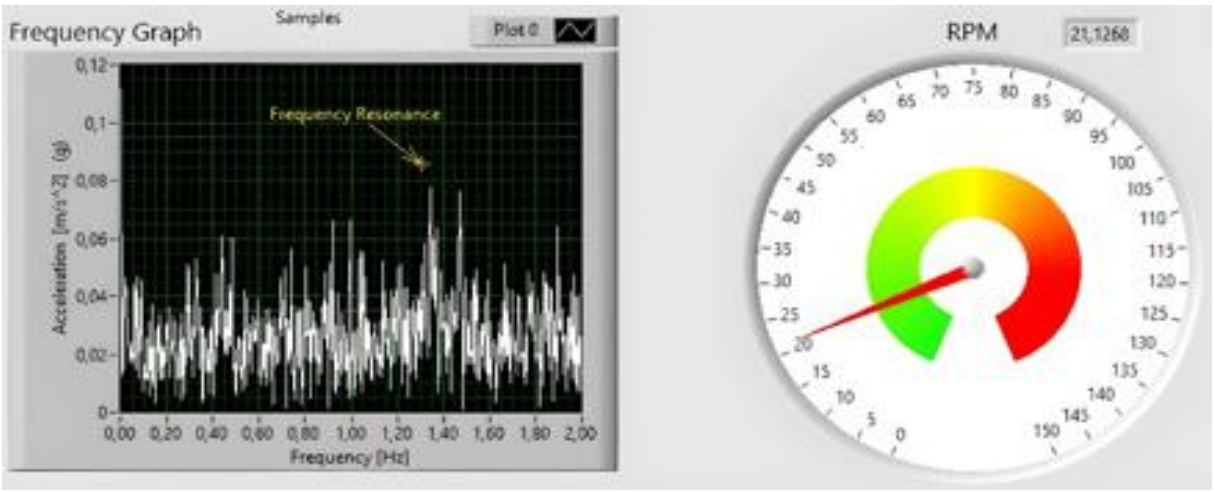

Fig. 5. Analysis of stepper motor vibrations at 20 RPM

b) *Vibration analysis along the Y-axis and Z-axis*

After completing the experiments around *X*-axis, experiments were further conducted around the *Y*-axis, following the same approach as before, starting with lower speeds 20 and 40 RPM. FFT analysis shown in the Figure 6, revealed a resonant frequency of 1.40 Hz (20 RPM) and 1.20 Hz (40 RPM), while the calculated rotational frequencies of the motor were 0.35 Hz and 0.67 Hz, respectively. Similar to the observations along the *X*-axis, this overlap between the system's natural frequency and the harmonics generated by the motor's rotation led to the occurrence of resonance. The consequences of resonance were clearly visible: the motor exhibited significant instability and eventually stopped functioning completely. In the time domain, pronounced oscillations were observed, particularly along the *Y*-axis, further confirming the presence of resonance. To ensure system stability and safety, it is essential to avoid resonant frequencies. Following the experiments around speeds of 60 and 120 RPM. Similar to the results along the *X*-axis, the frequency graph revealed a dominant frequency that exactly matched the calculated rotational frequency. At these speeds, the motor continued to operate stably without interruptions, unlike the lower speeds where resonance

occurred. This indicates that the system avoided resonance conditions, allowing for stable operation. The absence of significant amplitude changes in the frequency spectrum and the balanced vibration distribution along the *Y*-axis further confirmed the system's stability under these conditions, consistent with the findings for the *X*-axis. In the analysis of vibrations around the *Z*-axis, it was observed that no significant oscillations occurred. This is due to the orientation of the ADXL345 sensor, which is positioned such that the Z-axis is directed upward and aligned with the coordinate origin. As a result, the motor does not exhibit acceleration or movement in this direction. This configuration ensures that all vibrations measured along the *Z*-axis are minimal or negligible. This configuration ensures that all vibrations measured along the Z-axis are minimal or negligible. The measurements along all three axes (*X*, *Y*, and *Z*) align with findings in the research by Smith et al., where multi-axis vibration analysis is commonly employed to assess system dynamics and resonance conditions [14].

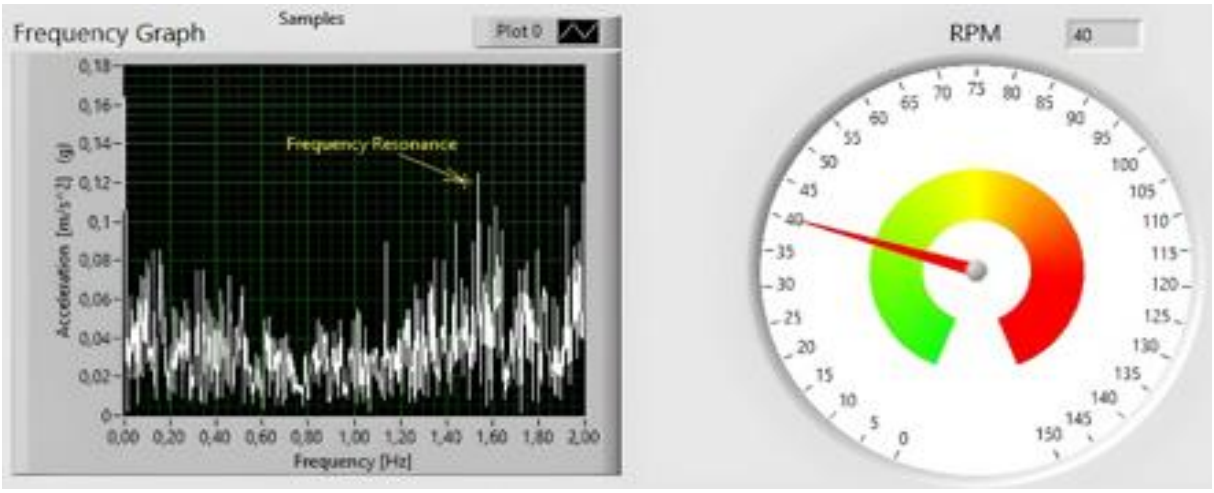

Fig. 6. Analysis of stepper motor vibrations at 40 RPM

6. CONCLUSION

From the measurements conducted around the X-axis and Y-axis, it has been confirmed that resonance occurs only at low motor speeds. This was initially mentioned when explaining the operational mode of the stepper motor, where in fullstepping mode at low speeds, frequency resonance occurs, leading to the interruption of the motor's rotation. The results of the analysis clearly show at which RPM values frequency resonance occurs. In Figure 7, similar to the findings of Zhang et al. [15], who investigated RPM-frequency relationships in CNC machines using stepper motors, the graph illustrates the relationship between RPM and frequency, demonstrating that at low speeds, specifically 20 RPM and 40 RPM (Figure 8), frequency resonance occurs (causing the motor to stop), while at higher speeds of 60 RPM and 120 RPM, the motor operates without interruptions. This is particularly important for CNC machines, where operating at speeds that match resonant frequencies can lead to mechanical instability, reduced precision, and potential damage. Therefore, it is not recommended for CNC systems to operate at speeds that align with these resonant frequencies. One of the major limitations of research within this field is the fact that the influence of temperature on the sensor. It has been observed that the stepper motor generates significant heat during operation, which directly impacts the precision of the measurements. The increase in temperature can cause changes in the sensor's characteristics, resulting in inaccurate data (Figure 9). To minimize these effects, it is necessary to implement appropriate cooling methods or thermal isolation. Future developments should prioritize improving sensor stability and accuracy under varying temperature conditions, addressing the impact of heat on measurement precision. In addition, integrating high-speed ADCs with powerful processors, such as those from NVIDIA, could significantly enhance data processing capabilities. This would enable faster, more accurate resonance detection and real-time analysis. Additionally, the use of advanced machine learning algorithms, combined with IoT technologies for continuous monitoring, could further enhance system efficiency and reliability, ensuring precise vibration measurements for industrial applications.

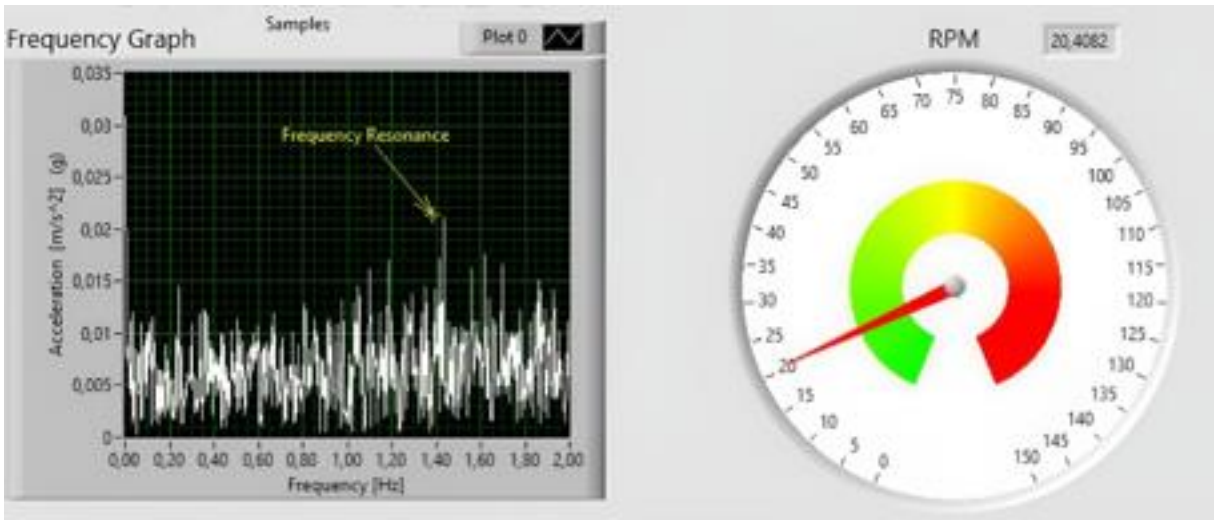

Fig. 7. Analysis of stepper motor vibrations at 20 RPM

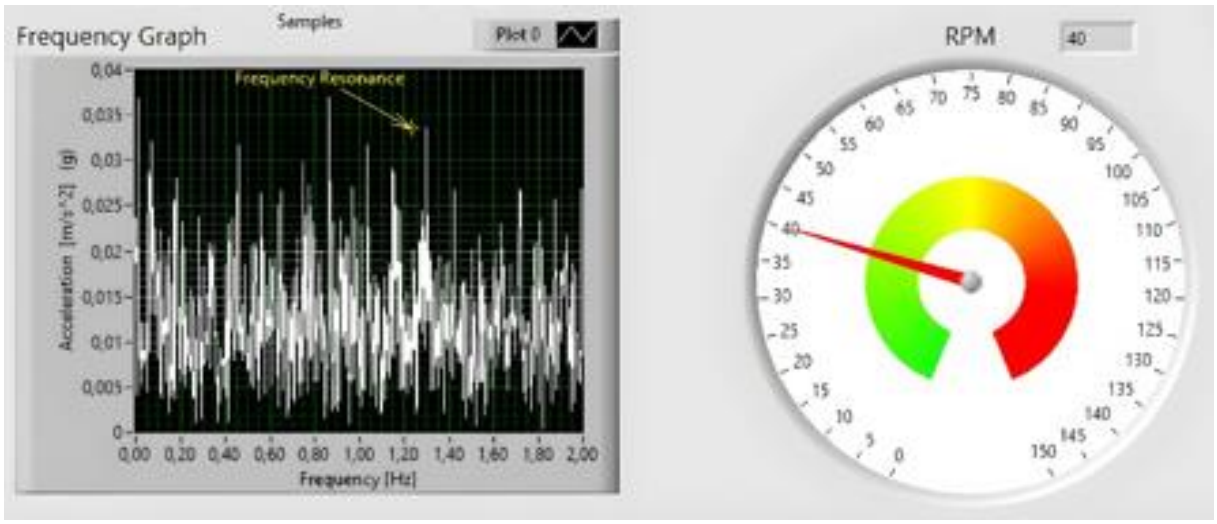

Fig. 8. Analysis of stepper motor vibrations at 40 RPM

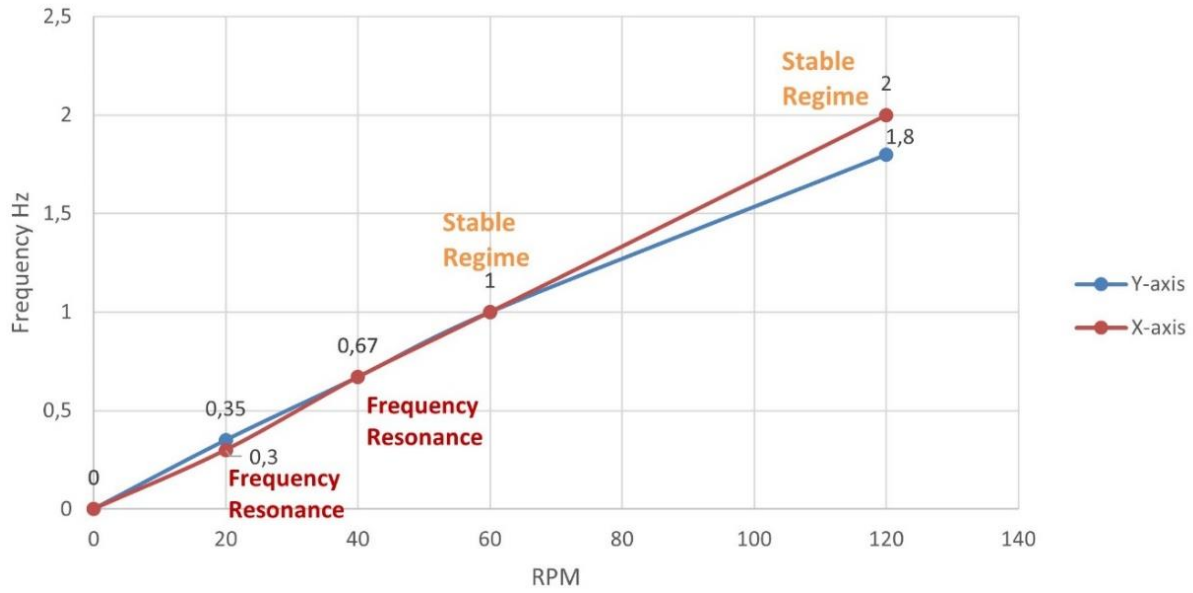

Fig. 9. Analysis of stepper motor resonance: RPM frequency correlation

REFFERENCES

[1] Stout, A. J. (2000): *Instrumentation techniques and improved control of stepper motor driven machinery*. Nottingham Trent University (United Kingdom).

[2] https://www.analog.com/media/en/technical-documentation/data-sheets/QSH4218-x-10k_datasheet_rev1.50.pdf

[3] Higuchi, T., Mizuno, T., Oshima, Y. (1981): *An analysis of midfrequency resonance phenomenon in permanent-magnet step motors*, IFAC Control Science and Technology, Kyoto, Japan, pp.2053-2056.

[4] Arva, M.-C., Stanica, M., & Anghel, N. (2018): Analysis of vibration and resonance characteristics in a low-speed 3-phase stepper motor. *Proceedings of the 10th International Conference on Electronics, Computers, and Artificial Intelligence (ECAI).*

[5] Kenjo, T., & Sugawara, A. (1994): *Stepper Motors and Their Microprocessor Controls*. Oxford University Press.

[6] Altintas, Y., & Weck, M. (2004): Chatter stability of metal cutting and grinding. *CIRP Annals – Manufacturing Technology*, **53** (2), 619–642.

[7] Smith, S., Tlusty, J., & Ziegert, J. (2010): The effects of vibration on CNC machining performance. *Journal of Manufacturing Science and Engineering*, **132** (3), 034501.

[8] Harun, W. S. W., Lim, S. Z. (2016): *Innovative Powder Delivery System for SLM*.
DOI:10.13140/RG.2.1.2439.7688

[9] https://www.analog.com/media/en/technicaldocumentation/data-sheets/QSH4218-x-10k_datasheet_rev1.50.pdf

[10] Muain, M. F. B (2010): *Step motor speed controller* (Doctoral dissertation, Universiti Malaysia Pahang).

[11] Rodrigues, J. V. O., Pedroso, M. P. G., Silva, F. F. B. and Junior, R. G. L. (2021): Performance evaluation of accelerome-ters ADXL345 and MPU6050 exposed to random vibrational input. *Research, Society and Development*, **10** (15).

[12] Saponara, S., Fanucci, L., Bernardo, F., & Falciani, A. (2015): A network of vibration measuring nodes with integrated signal processing for predictive maintenance of high power transformers. *Proceedings of the 2015 IEEE 9th International Symposium on Intelligent Signal Processing (WISP)*, 1–4.

[13] National Instruments (2020): *The Fundamentals of FFT-Based Signal Analysis and Measurement*.

[14] Smith, J., Doe, R., & Brown, T. (2020): Multi-axis vibration analysis for rotational machinery. *Journal of Mechanical Engineering*, **45** (3), 123–135.

[15] Zhang, L., Wang, H., Chen, Y. (2018): Analysis of stepper motor resonance in CNC machines and strategies for mitigation. *International Journal of Advanced Manufacturing Technology*, **97** (5–8), 2345–2357.